Neuroinformatics (2025) 23:27
https://doi.org/10.1007/s12021-025-09720-x

RESEARCH

Revealing the Multivariate Associations Between Autistic Traits and Principal Functional Connectome

Jong-eun Lee[1,2] · Kyoungseob Byeon[3] · Sunghun Kim[2,4] · Bo-yong Park[2,4] · Hyunjin Park[1,2]

Accepted: 24 February 2025

Abstract

Autism Spectrum Disorder (ASD) is a multifaceted neurodevelopmental condition characterized by a spectrum of behavioral and cognitive traits. As the characteristics of ASD are highly heterogeneous across individuals, a dimensional approach that overcomes the limitation of the categorical approach is preferred to reveal the symptomatology of ASD. Previous neuroimaging studies demonstrated strong links between large-scale brain networks and autism phenotypes. However, the existing studies have primarily focused on univariate association analysis, which limits our understanding of autism connectopathy. Using resting-state functional magnetic resonance imaging data from 309 participants (168 individuals with ASD and 141 typically developing controls) across a discovery dataset and two independent validation datasets, we identified multivariate associations between high-dimensional neuroimaging features and diverse phenotypic measures (20 or 7 measures). We generated low-dimensional representations of functional connectivity (i.e., gradients) and assessed their multivariate associations with autism-related phenotypes of social, behavioral, and cognitive problems using sparse canonical correlation analysis (SCCA). We selected three functional gradients that represented the cortical axes of the sensory-transmodal, motor-visual, and multiple demand-rests of the brain. The SCCA revealed multivariate associations between gradients and phenotypic measures, which were noted as linked dimensions. We identified three linked dimensions: the links between (1) the first gradient and social impairment, (2) the second and internalizing/externalizing problems, and (3) the third and metacognitive problems. Our findings were partially replicated in two independent validation datasets, indicating robustness. Multivariate association analysis linking high-dimensional neuroimaging and phenotypic features may offer promising avenues for establishing a dimensional approach to autism diagnosis.

Keywords Autism spectrum disorder · Functional gradient · Multivariate analysis · Sparse canonical correlation analysis

Introduction

Autism Spectrum Disorder (ASD) is a common neurodevelopmental condition characterized by atypical behavioral and cognitive traits (Hodges et al., 2020; Maenner, 2023). Individuals with ASD are characterized by difficulties in social interaction and communication along with repetitive behaviors or restricted interests (Masi et al., 2017). Diagnosis and intervention are challenging owing to the complexity of the condition. Indeed, psychiatric conditions such as Attention-Deficit/Hyperactivity Disorder (Lai et al., 2019), Major Depressive Disorder (Wichers et al., 2023), and anxiety (Vasa & Mazurek, 2015) are commonly observed in ASD diagnoses (Hours et al., 2022). Hence, a dimensional approach may be suitable for improving diagnostic reliability and formulating targeted interventions instead of a discrete classification of ASD.

Neuroimaging studies have substantially improved the understanding of ASD (Hernandez et al., 2015; Liloia et al., 2022). Using resting-state functional magnetic resonance imaging (rs-fMRI), which measures the spontaneous brain activity of cerebral blood flow (Biswal et al., 1995), previous studies have reported that the autistic brain is likely

✉ Hyunjin Park
hyunjinp@skku.edu

1 Department of Electrical and Computer Engineering, Sungkyunkwan University, Suwon, South Korea

2 Center for Neuroscience Imaging Research, Institute for Basic Science, Suwon, South Korea

3 Center for the Developing Brain, Child Mind Institute, New York, NY, USA

4 Department of Brain and Cognitive Engineering, Korea University, Seoul, South Korea

Published online: 01 April 2025

characterized by both hypoconnectivity (Assaf et al., 2010; Jones et al., 2010; Kennedy & Courchesne, 2008) and hyperconnectivity (Cerliani et al., 2015; Chien et al., 2015). Recently, a connectome gradient approach that generates low-dimensional principal components of connectivity using manifold learning has emerged (Margulies et al., 2016). This approach offers a new perspective for investigating the brain with continuously changing connectivity patterns within the brain hierarchy. Compared to directly analyzing high-dimensional connectivity matrices, functional gradients provide a low-dimensional representation of the brain's large-scale organization, capturing hierarchical transitions from unimodal sensory areas to higher-order transmodal association regions (Margulies et al., 2016). This hierarchy-based view is particularly relevant to ASD, which involves atypical perceptual processing, social-communicative challenges, and restricted interests. By focusing on these principal axes, we can more effectively investigate how ASD-related alterations might originate in lower-level sensory processing and reverberate through higher-order cognitive regions. Hong et al. adopted the gradient approach and showed shifts in functional gradients in individuals with ASD compared to typically developing (TD) controls, particularly in the default mode network (Hong et al., 2019), indicating atypicality in lower-level sensory/motor and higher-order default mode regions in ASD.

Most previous research on ASD was conducted based on a case–control design (Dichter, 2012; Hong et al., 2019; Lau et al., 2019; Park et al., 2021; Rasero et al., 2023) with a limited range of symptom data, thus potentially overlooking inter-individual variations in autistic traits within the ASD population (Bölte et al., 2008). To delineate the complexity of ASD symptoms, a comprehensive framework incorporating high-dimensional neuroimaging features and a variety of phenotypic measures, such as metacognitive problems or internalizing behaviors, is necessary. This dimensional analysis provides a more holistic insight into psychiatry by considering a spectrum of phenotypic variations and their interactions with neuroimaging data (Xia et al., 2018; Yahata et al., 2016). A seminal study by Xia et al. employed sparse canonical correlation analysis (SCCA) across multiple brain regions and phenotypic scores to identify the important markers of various psychiatric conditions (Xia et al., 2018). SCCA is a classical method for identifying multivariate associations between two high-dimensional datasets (i.e., connectome and various phenotypes) in a sparse sample setting and is thus well suited for investigating studies based on dimensional approaches (Witten et al., 2009).

In this study, we aimed to uncover multivariate associations between high-dimensional functional connectome gradients and a diverse array of phenotypic items to delineate the dimensions of ASD symptoms. To this end, we applied SCCA to identify interactions between neuroimaging patterns and autistic traits. The results of our framework may serve as a blueprint for aiding ASD diagnosis and formulating targeted interventions.

Methods

Participants

We studied the MRI and phenotypic data from the Autism Brain Imaging Data Exchange initiatives (ABIDE I and II) (Di Martino et al., 2014, 2017). To analyze the wide range of symptoms associated with autism, we included not only autism-specific measures (i.e., Social Responsiveness Scale; SRS) (Constantino, 2013; Constantino & Gruber, 2005) but also broader psychometric assessments (i.e., Behavior Rating Inventory of Executive Function and Child Behavior Checklist Ages 6–18; BRIEF and CBCL) (Achenbach & Rescorla, 2001; Gioia et al., 2015) applicable to the general population. Only participants with complete data for all three assessments were included. A full list of symptom evaluations is given in the next section. We then excluded participants who failed one or more of the following MRI quality inclusion criteria: *i*) mean framewise displacement less than 0.5 mm, *ii*) satisfactory surface reconstruction, and *iii*) an acceptable seed-based connectivity pattern across three networks (default mode network, dorsal attention network, and salience network). These screening processes resulted in a final sample of 309 individuals from the ABDIE I and II datasets. The data used for discovery were sourced from a subsample of ABIDE II, resulting in 177 individuals from two sites: (1) Georgetown University (GU, 29/44, ASD/controls) and (2) Kennedy Krieger Institute (KKI, 25/79, ASD/controls). Two independent datasets (Validation 1 and 2) were curated for validation analyses, both from New Your University Langone Medical Center (NYU) containing subsamples of ABIDE II (53/18, ASD/controls) and ABIDE I (61 ASD), respectively. The demographic information of the three datasets is presented in Table 1.

Phenotypic Data

In the Discovery and Validation 1 dataset, autistic symptoms were evaluated through in-person interviews using the SRS, BRIEF, and CBCL. These scores assess five categories of autistic symptoms: social impairment, behavioral problems, metacognitive problems, internalizing behaviors, and externalizing behavioral problems. In the Validation 2 dataset, autistic symptoms were evaluated using the following interviews: the Autism Diagnostic Interview-Revised (ADI-R) (Lord et al., 1994), Autism Diagnostic Observation Schedule (ADOS) (Lord et al., 2012), and Vineland Adaptive Behavior Scales

Table 1 Demographic information of study participants

		Total	Discovery	Validation 1	Validation 2	Discovery vs. Validation 1 statistics (p-value)	Discovery vs. Validation 2 statistics (p-value)
N		309	177	71	61		
Diagnosis	ASD	168	54	53	61	38.47 ($p < 0.01$)	84.97 ($p < 0.01$)
	TD	141	123	18	0		
Sex	Male	230	112	66	54	20.60 ($p < 0.01$)	12.54 ($p < 0.01$)
	Female	79	65	5	7		
Age (Mean ± SD)		10.82 ± 3.35	10.52 ± 1.45	8.99 ± 2.26	13.83 ± 5.68	5.31 ($p < 0.01$)	−4.50 ($p < 0.01$)
Mean FD [mm]		0.17 ± 0.08	0.18 ± 0.09	0.16 ± 0.08	0.14 ± 0.06	1.66 ($p = 0.10$)	3.83 ($p < 0.01$)
SRS total		57.67 ± 43.81	39.50 ± 40.88	74.13 ± 37.97	91.23 ± 29.37	−6.35 ($p < 0.01$)	−10.65 ($p < 0.01$)
Handedness	Right	206	158	48		12.59 ($p < 0.01$)	
	Left	15	11	4			
	Mixed	20	8	12			

The p-values for diagnosis, sex, and handedness were calculated using the chi-square test, whereas the p-values for age, mean FD, and SRS total were calculated using two-sample t-tests. Handedness data were not collected in the Validation 2 samples and therefore do not appear in the table

ASD, autism spectrum disorder; TD, typically developing control; SD, standard deviation; FD, framewise displacement; SRS, social responsiveness scale

(VINELAND) (Sparrow & Cicchetti, 1989). However, these scores were not identical across Discovery, Validation 1, and Validation 2 datasets. Only the social impairment and behavior problem categories were available for the Validation 2 dataset (Table 2). Thus, we compared phenotypic scores in the same category. This approach was adopted to ensure that the phenotypic scores could be fairly compared between datasets at the abstract level.

Table 2 Phenotype data mapped to five categories

Category	Discovery & Validation 1 dataset	Validation 2 dataset
Social impairment	SRS: Social awareness	ADI-R: Reciprocal social interaction
	SRS: Social cognition	ADOS: Social
	SRS: Social communication	VINELAND: Interpersonal relationships
	SRS: Social motivation	VINELAND: Play and leisure time
		VINELAND: Coping skills
Behavior problem	BRIEF: Inhibit	ADI-R: RRBs
	BRIEF: Shift	ADOS: Stereotyped behaviors
	BRIEF: Emotional control	
Metacognition problem	BRIEF: Initiate	
	BRIEF: Working memory	
	BRIEF: Plan/Organize	
	BRIEF: Organization of materials	
	BRIEF: Monitor	
Internalizing behavior	CBCL: Anxious/Depressed	
	CBCL: Withdrawn/Depressed	
	CBCL: Somatic complaints	
Externalizing behavior	CBCL: Social problems	
	CBCL: Thought problems	
	CBCL: Attention problems	
	CBCL: Rule-breaking behaviors	
	CBCL: Aggressive behaviors	

SRS, social response scale; BRIEF, Behavior Rating Inventory of Executive Function; CBCL, Child Behavior Checklist Ages 6–18; ADI-R, Autism Diagnostic Interview-Revised; ADOS, Autism Diagnostic Observation Schedule; VINELAND, Vineland Adaptive Behavior Scales; RRB, Restricted and repetitive behavior

MRI Data Acquisition

Both T1-weighted (T1w) and rs-fMRI data were sourced from all involved sites. Images were acquired using 3 T scanners from Siemens (GU: TrioTim scanner; NYU: Allegra scanner) and Philips (KKI). For the GU, the T1w data were acquired using a 3D-MPRAGE sequence (repetition time [TR] = 2530 ms; echo time [TE] = 3.5 ms; T1 = 1100 ms; flip angle = 7°; matrix = 256 × 256; 1.0 × 1.0 × 1.0 mm^3 voxels) and rs-fMRI using 2D-EPI (TR = 2000 ms; TE = 30 ms; flip angle = 90°; matrix = 64 × 64; 154 volumes; 3.0 × 3.0 × 2.5 mm^3 voxels). NYU data were acquired using 3DTurboFLASH for T1w (TR = 2530 ms; TE = 3.25 ms; TI = 1100 ms; flip angle = 7°; matrix = 256 × 256; 1.3 × 1.0 × 1.3 mm^3 voxels) and 2D-EPI for rs-fMRI (TR = 2000 ms; TE = 15 ms; flip angle = 90°; matrix = 80 × 80; 180 volumes, 3.0 × 3.0 × 4.0 mm^3 voxels). KKI data were acquired using 3D-MPRAGE for T1w (TR = 3500 ms; TE = 3.7 ms; TI = 1000 ms; flip angle = 8°; matrix = 256 × 200; 1.0 × 1.0 × 1.0 mm^3 voxels) and 2D-EPI for rs-fMRI (TR = 2500 ms; TE = 30 ms; flip angle = 75°; matrix = 84 × 81; 128/156/162 volumes, 3.0 × 3.0 × 3.0 mm^3 voxels).

MRI Preprocessing

The MRI data were preprocessed using fMRIPrep (Esteban et al., 2019), an open-source tool designed for fMRI data preprocessing. First, the T1w image was corrected for intensity non-uniformity using N4BiasFieldCorrection (Tustison et al., 2010), which served as the T1w-reference for the entire workflow. Non-brain tissues were removed from the T1w-reference image (Avants et al., 2008), and the white matter, gray matter, and cerebrospinal fluid were segmented (FSL v5.0.9) (Zhang et al., 2001). Cortical surfaces were reconstructed using recon-all (FreeSurfer v6.0.1) (Fischl, 2012), and the brain mask was refined by integrating ANT- and FreeSurfer-derived cortical gray matter segmentations using a custom variation of the Mindboggle approach (Klein et al., 2017). For rs-fMRI, we first estimated six head motion parameters of rotations and translations. Slice timing correction was performed using the 3dTshift from AFNI (Cox & Hyde, 1997). Subsequently, the fMRI and T1w-reference data were co-registered using boundary-based registration (Greve & Fischl, 2009). Volume-to-surface mapping was performed using the Ciftify toolbox (version 2.3.3) (Dickie et al., 2019). Specifically, rs-fMRI was resampled to the Conte69 32 k surface mesh, and surface-based smoothing with a full-width at half-maximum of 3 mm was applied (Glasser et al., 2013). To reduce the computational load, the data were resampled to a Conte69 10 k mesh.

Connectome Gradient Generation

We constructed a functional connectivity matrix by calculating the Pearson correlations of the time series between different brain regions defined using Schaefer 200 surface-based parcellations (Schaefer et al., 2018) (Fig. 1 a-b). Each matrix was

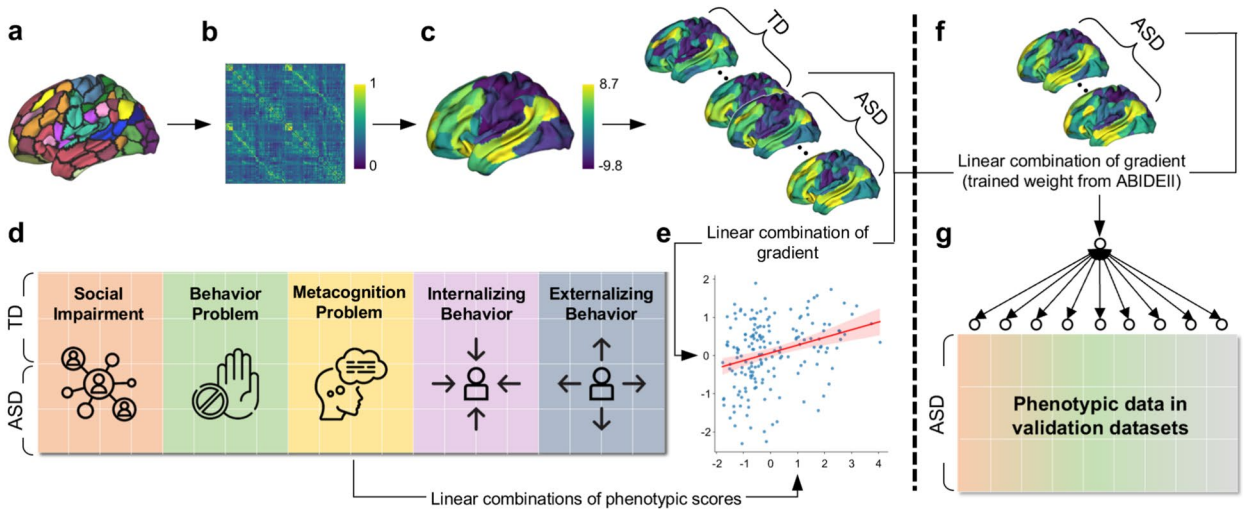

Fig. 1 Overview of the methodological procedure. **a.** After preprocessing, functional time series were extracted from 200 pre-specified brain regions (Schaefer et al., 2018). **b.** For each subject, a 200 × 200 functional connectivity matrix was constructed. **c.** A functional gradient was derived from the individual's functional connectivity. **d.** Phenotypic data of five categories of autistic symptoms were assessed: social impairment, behavior problems, metacognition problems, internalizing behavior, and externalizing behavior problems. **e.** SCCA identified a multivariate association (noted as a linked dimension) between neuroimaging and phenotypic scores. **f.** The canonical neuroimaging score was computed by a linear combination of the functional gradient of the validation set and the canonical weights of the discovery set. **g.** The canonical score was correlated with various phenotypic scores of the validation set. Procedures (a)-(e) occur in the discovery set, whereas procedures (f) and (g) occur in the validation set

200 × 200, where the (*i*,*j*)-th element reflected the correlation between region *i* and region *j*. The correlation coefficients were z-transformed to normalize the distribution of these correlation values. Next, the functional connectivity matrix was thresholded, leaving only the top 10% of the weighted connections per row, focusing on the most robust relationships. Subsequently, we calculated a cosine similarity matrix to capture the similarity in connectivity profiles across regions and applied diffusion map embedding implemented in the BrainSpace toolbox (Vos de Wael et al., 2020) to generate low-dimensional representations, referred to as "functional gradients" (Fig. 1c). Individual gradients were aligned to the template using Procrusted rotation to ensure comparability (Langs et al., 2015; Vos de Wael et al., 2020). The gradient template was derived from an average connectivity matrix of healthy subjects, provided by the ENIGMA toolbox (Larivière et al., 2021). To correct the site effects, individual gradients were harmonized using the combat method (Fortin et al., 2018). Following site harmonization, the confounding factors of age and sex were regressed out from the gradients.

Multivariate association analysis linking neuroimaging and phenotypic features

We opted to use the SCCA technique to identify links between functional gradients and autism-related phenotypic scores. Canonical correlation analysis (CCA) is a standard method used to identify multivariate associations between two types of high-dimensional data (Hotelling, 1992). SCCA is a variant of CCA designed to identify a sparse array of loading vectors in two sets of features through a regularization technique (Witten et al., 2009). In low-sample scenarios, the SCCA may be more suitable than the traditional CCA because it mitigates the overfitting issue (Zhuang et al., 2020). In SCCA, given two feature matrices, $X_{n\times p}$(e.g., functional gradients) and $Y_{n\times q}$(e.g., phenotypic scores), where 'n' represents the number of observations (e.g., participants), 'p' and 'q' denote the number of features. SCCA aims to find loading vectors 'u and 'v' that optimize the correlation between Xu and Yv. From a mathematical perspective, this optimization problem can be expressed as

$$maximize(Xu)^T Yv, \text{ subject to } \|u\|_2^2 \le 1, \|v\|_2^2 \le 1, \|u\|_1 \le c_1, \|v\|_1 \le c_2$$

The penalty parameters of L^1 norm, namely c_1 and c_2, are user-defined parameters that require fine-tuning. This tuning was executed via stratified five-fold cross-validation, while maintaining the ratio between ASD and TD, wherein the SCCA model constructed from the training fold was tested on the left-out test fold using various (c_1,c_2) values in 0.3 increments of 0.3 and 0.9. To determine the tuning parameters, the average canonical correlation across five test folds was used. The entire process was repeated 50 times, and the final tuning parameters were the average of 50 trials. Although SCCA can, in principle, produce multiple modes, we focused on the first (dominant) mode in our analyses, as it reflects the strongest linear association between the two feature sets. Consequently, the one-dimensional loading vectors thus identified 'u' (for neuroimaging; 200 × 1) and 'v' (for phenotypes; 20 × 1), which indicate the link bridging the high-dimensional neuroimaging and phenotypic scores (Fig. 1e). The two vectors show the multivariate associations between two data types and thus are noted as the *"linked dimension"*. We utilized the bootstrap resampling procedure (80%; n = 1000) to estimate the distribution of canonical correlations. From these distributions, we calculated 95% confidence intervals (CIs) using a percentile-based approach and deemed the correlations significant if their intervals did not include zero. Then, the loading vectors derived from resampled data were averaged and used for further analysis.

Validation of the Linked Dimension

An independent validation was performed using two separate validation datasets (Validation 1 and Validation 2). Validation 1 employs the same phenotypic battery as the discovery dataset, whereas Validation 2 has a mismatch in phenotypic scores. To apply a consistent validation method across both datasets, we correlated a canonical neuroimaging score (i.e., the linear combination of the loading vector and functional gradients) with the phenotypic scores available in each validation dataset (Fig. 1f-g). The canonical neuroimaging score was computed as the linear combination of the functional gradient of the validation set with the neuroimaging loading vector 'u' derived from the discovery set (i.e., Xu). We then correlated this score with individual phenotypic scores to examine whether the canonical score from neuroimaging was associated with similar phenotypic scores in the validation set.

Visualization of Gradients

To elucidate the differences in functional gradients among autistic individuals, we employed two visualization techniques. First, we compared histograms of the functional gradients between the top 10% and bottom 10% of canonical phenotypic scores (i.e., Yv) for G1, G2, and G3 from our discovery dataset. We performed Kolmogorov–Smirnov (KS) tests (Massey, 1951) on these histograms to quantify differences in distribution between individuals with higher and lower symptom severity. Additionally, for a more comprehensive understanding, we mapped all gradient values to a 3D scatter plot. This plot's spatial positions corresponded to gradient values, with each data point color-coded using a scheme based on its canonical phenotypic scores (Red: G1, Green: G2, Blue: G3). Each dimension's canonical

phenotypic score is mapped onto its respective color channel and the overall intensity of each data point becomes darker with higher symptom severity. Consequently, participants with milder overall symptoms appear lighter in color, whereas those with more severe symptoms appear darker, facilitating the interpretation of how each gradient position relates to multidimensional phenotype scores.

Discriminability of Linked Dimensions

To assess the ability of each linked dimension to distinguish individuals with ASD from those with TD, we compared the canonical neuroimaging scores (see the previous section on multivariate association) between the two groups. The significance of these comparisons was reported using p-values obtained from two-sample t-tests, and multiple comparisons across gradients were corrected using false discovery rate (FDR). For this analysis, we used a sample of 168 individuals with ASD and 141 TD from the discovery and validation datasets. We also examined how comorbidity might influence these canonical neuroimaging scores. For participants in the discovery dataset who had documented comorbid diagnoses, we compared the canonical neuroimaging scores of individuals with ASD alone to those with ASD plus a comorbid ADHD diagnosis using two-sample t-tests. This approach enabled us to determine whether comorbidity was associated with distinct alterations in any of the linked dimensions.

Results

Functional Connectome Gradients

Three functional gradients were generated, accounting for approximately 51% of the information in the functional connectivity matrix (Fig. 2a) in the Discovery dataset. The number of components was selected using the elbow method and interpretability of the spatial patterns. The three functional gradients (G1, G2, and G3) were largely consistent with previous findings based on the Human Connectome Project (HCP) dataset (Margulies et al., 2016). G1 extended from the primary sensory/motor to the association cortices, G2 unfolded from the somatomotor to the visual regions, while G3 stretched from the task-negative systems to multiple demand networks (Margulies et al., 2016) (Fig. 2b).

Linked Dimension of Autistic Traits and Functional Gradients

We identified multivariate associations of autistic traits, denoted as linked dimensions, with three functional gradients. Each gradient was fitted separately, resulting in a unique association. The phenotypic part of the linked dimension is a vector that allows for flexible assignment to different categories of phenotypic features. However, all three dimensions were characterized by distinct phenotypic features. The dominant phenotypic feature category was used to assign labels to the linked dimensions. For each gradient, only the first mode of SCCA was analyzed as the linked dimension, as it explained most variance (G1: 10.8%, G2: 15.2%, G3: 20.4%).

Social Impairment Dimension Linked to G1

Utilizing parameter tuning of $c_1 = 0.3$ and $c_2 = 0.3$, we identified a latent dimension linking phenotypes to G1 with a canonical correlation of 0.31 (Fig. 3a). A percentile-based bootstrap procedure yielded a 95% confidence interval of [0.23–0.37] indicating that the correlation was significantly different from zero. The canonical neuroimaging score of G1 was primarily associated with social impairment. Notably, social awareness (e.g., "Is aware of what others are thinking"), social cognition (e.g., "Doesn't recognize when others are trying to take advantage of him or her"), and social motivation (e.g.,

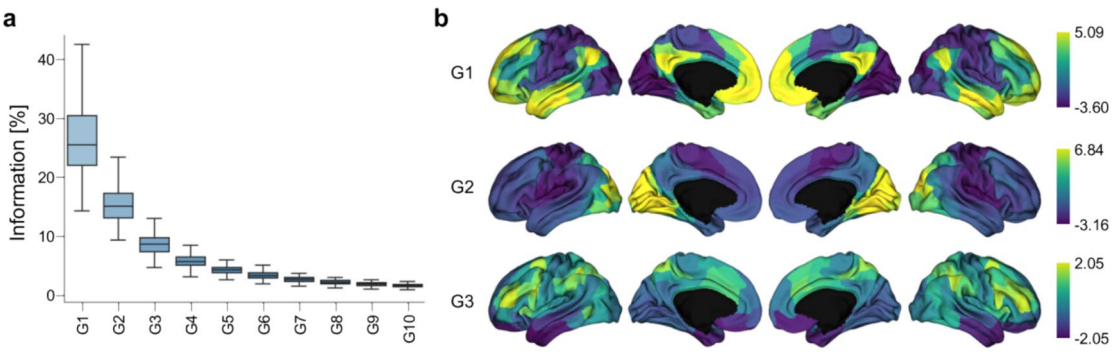

Fig. 2 Functional connectome gradients. **a.** Scree plot showing the information accounted for by the gradients. **b.** Spatial patterns of the generated gradients G1, G2, and G3

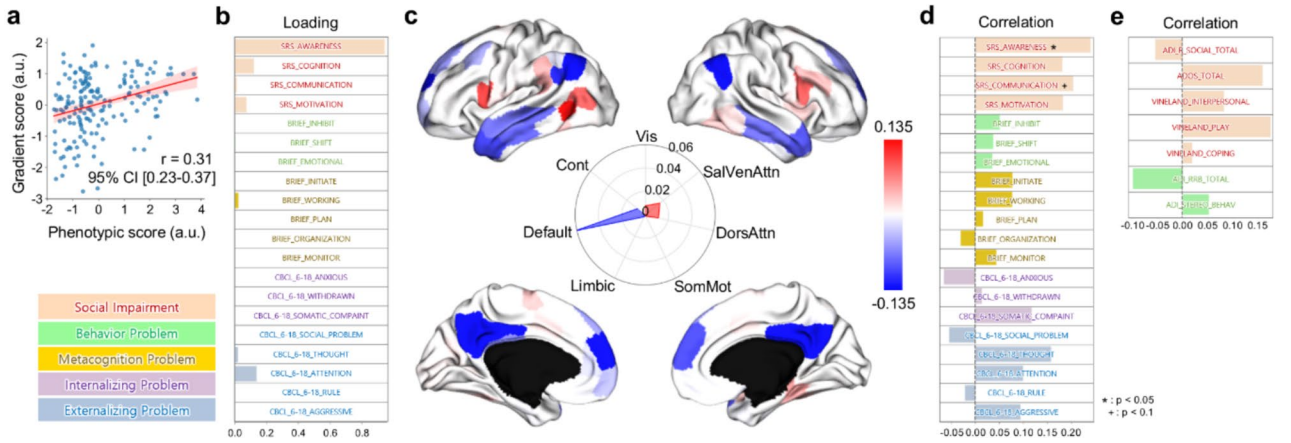

Fig. 3 Social impairment dimension linked to G1. **a.** Scatter plot of the correlation between phenotypic and canonical neuroimaging scores. **b.** Loading vector of phenotypic scores. **c.** Loading vector of G1. **d.** Univariate correlation coefficient with canonical neuroimaging scores and phenotypic scores in Validation 1 dataset. **e.** Univariate correlation coefficient with canonical neuroimaging scores and phenotypic scores in Validation 2 dataset

"Would rather be alone than with others") showed dominant weights within this category (Fig. 3b). Stratifying the loading vector of G1 according to a predefined network organization (Thomas Yeo et al., 2011), a noticeable decrease was observed in the default mode and control networks (Fig. 3c). We used two validation datasets for G1. In Validation 1, SRS_AWARENESS was significantly correlated with the G1 canonical neuroimaging score ($r = 0.24$, $p = 0.047$), reflecting the strong weighting of this score in the G1 loading vector and SRS_COMMUNICATION showed a trend-level correlation ($r = 0.20$, $p = 0.09$) (Fig. 3d). In Validation 2, the social category in ADOS ($r = 0.165$, $p = 0.204$ and the socialization subscore of VINELAND ($r = 0.174$, $p = 0.180$) showed moderate correlations (Fig. 3e). Although these correlations did not reach significance, their direction and relative magnitudes were generally consistent with the discovery set, with the strongest effects in the social domain. For the behavior problem measures, the correlations were negative or smaller (e.g., ADI_RRB: $r = -0.10$, $p = 0.44$; ADOS_STEREO_BEHAV: $r = 0.05$, $p = 0.69$). These findings support the notion that the G1-linked dimension reflects social impairments across multiple datasets.

Internalizing/Externalizing Problem Dimension Linked to G2

Utilizing the parameter tuning of $c_1 = 0.3$ and $c_2 = 0.9$, we discovered a latent dimension linking phenotypes to G2 with a canonical correlation of 0.28 (Fig. 4a). A

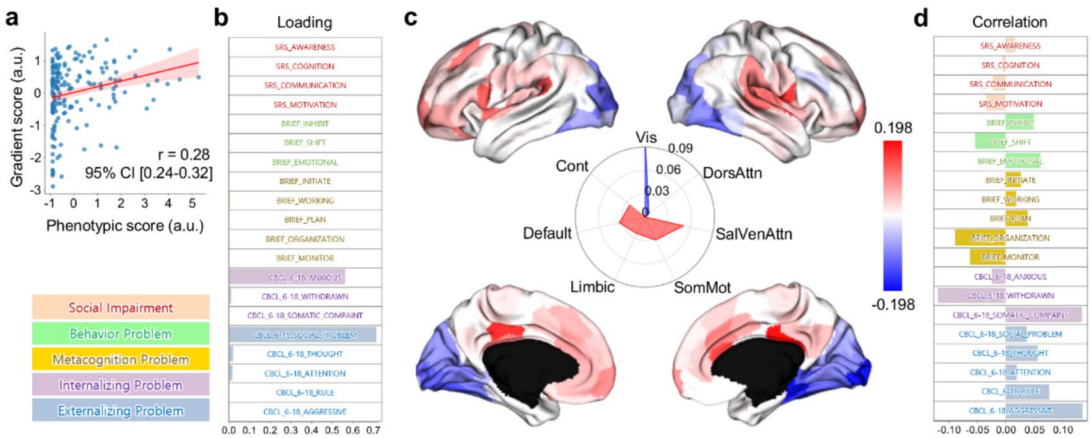

Fig. 4 Internalizing/Externalizing problem dimension linked to G2. **a.** Scatter plot of the correlation between phenotypic and canonical neuroimaging scores. **b.** Loading vector of phenotypic scores. **c.** Loading vector of G2. **d.** Univariate correlation coefficient with canonical neuroimaging scores and phenotypic scores in Validation 1 dataset

percentile-based bootstrap procedure yielded a 95% confidence interval of [0.24–0.32], indicating that the correlation was significantly different from zero. The canonical neuroimaging score of G2 was highly correlated with anxiety and social problem scores for internalizing and externalizing behaviors (Fig. 4b). In the validation analysis using Validation 2, the largest correlations remained concentrated in the domain of internalizing (e.g., CBCL_6-18_SOMATIC_COMPLAINT, r = 0.14, p = 0.26) and externalizing behaviors (e.g., CBCL_6-18_AGGRESSIVE, r = 0.14, p = 0.25) (Fig. 4d). However, CBCL_6-18_WITHDRAWN showed a moderate negative correlation (r = −0.12, p = 0.33), which limits the generalizability of the findings. Notably, we observed a marked decrease in the visual network (visual central and visual peripheral networks), whereas an increase was apparent in all seven networks, except for the visual and dorsal attention networks (Fig. 4c).

Metacognition Problem Dimension Linked to G3

Utilizing the parameter values $c_1 = 0.6$ and $c_2 = 0.3$, we identified a latent linked dimension with a canonical correlation of 0.40 (95% CI [0.26–0.45]) relating phenotypes to G3 (Fig. 5.a). In the validation analysis using Validation 2, SRS_COMMUNICATION (r = 0.30, p = 0.025), SRS_MOTIVATION (r = 0.34, p = 0.011), SRS_COGNITION (r = 0.25, p = 0.07), and BRIEF_WORKING (r = 0.24, p = 0.07) showed dominant correlations with the G3 canonical neuroimaging score, aligning with the social and metacognitive emphasis in the loading patterns (Fig. 5d). These scores were primarily related to the default mode regions (Fig. 5c).

Global Shrinkage Patterns of Gradients in Autistic Individuals

In all three gradients, a global shrinkage pattern was observed in the top 10% of the canonical phenotypical scores, especially with an increased middle portion of the histogram (Fig. 6a). Additionally, the KS test comparing the top 10% and bottom 10% of participants in each gradient confirmed significant differences for G1 (KS statistic = 0.064, p < 0.01), G2 (KS statistic = 0.090, p < 0.01), and G3 (KS statistic = 0.050, p < 0.01), indicating that individuals with higher phenotypic scores (i.e., worse symptoms) show notably different gradient distributions. This trend implies that those with pronounced social impairment (falling within the top 10% of canonical phenotypical scores for G1) tend to have gradient values near zero more frequently than their counterparts with milder impairments. Furthermore, the 3D scatter plot exhibited that participants with more pronounced autistic traits (vivid or dark dots) tended to cluster inward, showing shrinkage patterns consistent with previous studies (Hong et al., 2019) (Fig. 6b).

Discriminability of Linked Dimensions

The clinical implications of the three identified linked dimensions related to autistic phenotypes were demonstrated by assessing the ability of canonical neuroimaging scores to distinguish between the ASD and TD groups (Fig. 7). We found that the canonical scores of G1 (t = 2.795, $p_{FDR} < 0.01$) and G3 (t = 3.421, $p_{FDR} < 0.01$) were significantly different between the groups, whereas those of G2 showed moderate differences (t = 1.550, $p_{FDR} = 0.06$). In addition, we explored

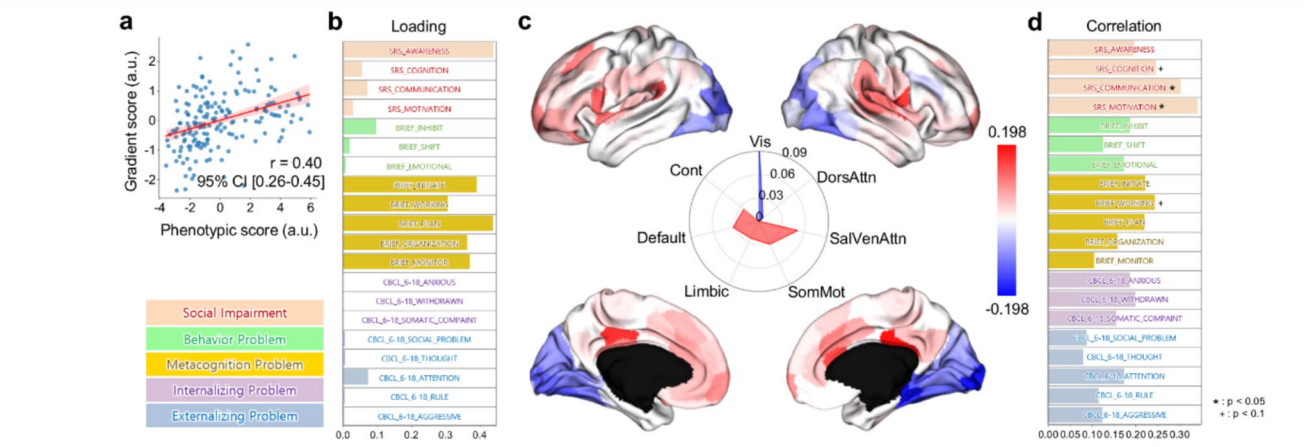

Fig. 5 Metacognition problem dimension linked to G3. **a.** Scatter plot of the correlation between phenotypic and canonical neuroimaging scores. **b.** Loading vector of phenotypic scores. **c.** Loading vector of G3. **d.** Univariate correlation coefficient with canonical neuroimaging scores and phenotypic scores in Validation 1 dataset

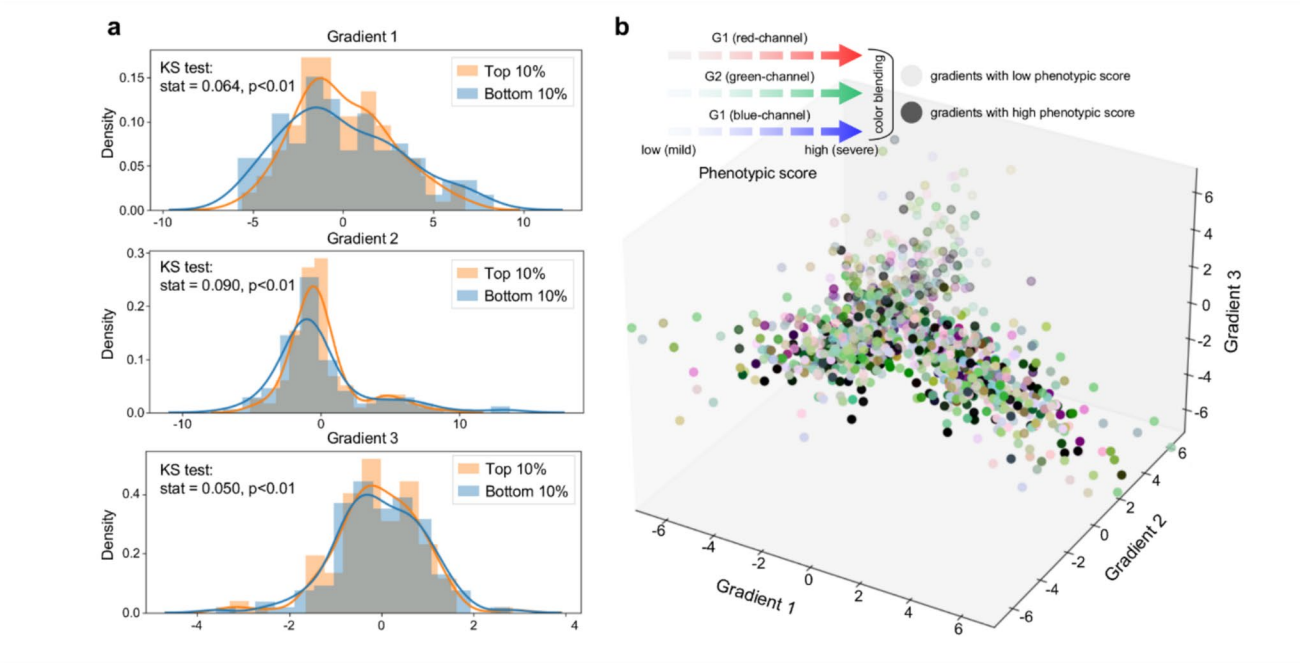

Fig. 6 Gradient patterns with respect to different levels of canonical phenotypical scores. a. Averaged gradient histograms of the top 10% and bottom 10% by canonical phenotypic score. b. 3D scatter plot of 3 gradients with RGB color mapping. Canonical phenotypic scores (i.e., G1, G2, and G3) are mapped onto red, green, and blue channels, where the overall intensity of each data point becomes darker with higher symptom severity. Consequently, participants with milder overall symptoms appear lighter in color, whereas those with more severe symptoms appear darker

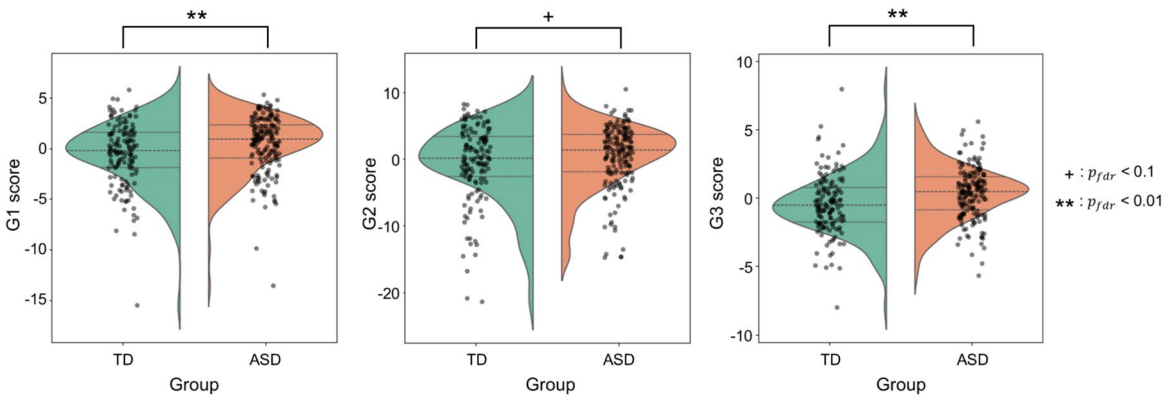

Fig. 7 Between-group differences in the canonical neuroimaging scores. Features that showed significant differences are marked with asterisks. Abbreviation: FDR, false discovery rate

how comorbidity may affect these canonical neuroimaging scores in individuals with ASD. Among the 54 ASD participants in the discovery dataset, 23 had documented comorbidities. Of these, 17 were comorbid with ADHD, 2 had anxiety disorder, 2 had oppositional defiant disorder, 1 had simple phobia, and 2 had major depressive disorder. ADHD was the most frequently observed comorbidity, consistent with clinical trends (Hours et al., 2022). A comparison of canonical neuroimaging scores revealed that those with comorbid ADHD exhibited significantly higher G1 (the dimension linked to social impairment) scores than those with ASD alone (0.66 vs. 0.21; t = 2.17, p = 0.03). In contrast, no significant differences emerged for G2 (0.30 vs. 0.14; t = 0.66, p = 0.51) or G3 (0.60 vs. 0.24; t = 1.49, p = 0.14).

Discussions

Individuals with psychiatric conditions often have comorbidities; therefore, a dimensional approach is preferred over conventional categorical approaches. To reveal the dimensional characteristics of functional brain organization in individuals with ASD, we performed a multivariate association analysis of SCCA, linking multiple functional gradients and various autism-related phenotypic measures. We identified three linked dimensions related to social impairment, internalization/externalizing behaviors, and metacognitive problems. These linked dimensions demonstrate the discriminative ability to diagnose ASD.

We delineated the functional brain organization using the gradient approach (Margulies et al., 2016). This technique enabled us to assess the spatial patterns of the cortical hierarchy and its shifts along the cortical surface according to disease state. Similar to previous work on normative and ASD populations (Hong et al., 2019; Margulies et al., 2016), we identified the representative cortical axes of sensory-transmodal, motor-visual, and multiple demand-task negative systems. The pattern of shrinkage along each axis was associated with distinct autistic traits (Fig. 6). Notably, the sensory-transmodal axis (G1) was associated with social impairment, highlighting the default mode networks. The identified regions are key players in evaluating one's emotional state during social interactions (Schulte-Rüther et al., 2007), and individuals with autism show abnormal functional connectivity in these regions during active cognitive processes (e.g., theory of mind) (Assaf et al., 2010). Moreover, a previous study using the gradient technique showed significant shifts in the functional connectome organization in the default mode network in individuals with ASD, again emphasizing the vulnerability of the network in autism connectopathy (Hong et al., 2019). The second gradient (G2) highlighted the associations between altered connectivity in the visual regions and internalizing and externalizing behavioral problems. This might be associated with 'sensory-first accounts' of autism, explaining that the irregular establishment of sensory circuits could potentially influence the maturation of higher-order cognitive control systems related to social interaction and communication skills (Robertson & Baron-Cohen, 2017). Impaired visual sensory processing has been observed in individuals with ASD (Marco et al., 2012). The third gradient (G3) was associated with metacognition, and the effect was dominated by the prefrontal cortex. Metacognition is a higher-order thinking skill crucial for enhancing the efficacy of decision-making processes. It has been shown that the ability of metacognition is highly associated with neural signaling computation in the prefrontal cortex, where the sensory signals are transmitted to the prefrontal cortex and make judgments after incorporating perceptual and non-perceptual factors (Shekhar & Rahnev, 2018). Indeed, patients with frontal lobe damage show impaired metacognitive abilities (Fleming & Dolan, 2012), indicating the pivotal role of higher-order cognitive control functions of the prefrontal cortex.

Using a dimensional approach, many functional connections that cannot be discovered with atypicality in a case–control design can be found (Buch et al., 2023). Our multivariate association design complemented previous work by considering the covariates of phenotypic scores, thus revealing the complex interplay between different phenotypic factors and their combined impact on brain hierarchy. For example, changes in ventral attention at G1, which reflects the unimodal-transmodal axis, are a relatively unexplored area of social impairment research in ASD. Furthermore, the linked dimension of G2 confirmed that the visual region is critical for a unified explanation of internalizing/externalizing behaviors.

One of the primary limitations of our study is the imbalance in demographic information between the discovery and validation datasets. The differences in the diagnosis ratio, sex, and age between the two datasets may have introduced bias into our findings. Furthermore, residual differences in the diagnosis ratio, mean FD, SRS total scores, and handedness remain even after regressing out key confounds of age and sex from the functional gradients. In addition, the absence of corresponding phenotypic categories in the validation dataset poses a challenge. This limitation prevented us from fully validating our findings and may have led to an incomplete understanding of the relationship between neuroimaging patterns and autistic traits. Future studies should aim to include a more comprehensive set of phenotypic categories in the validation dataset to ensure a more robust validation of the findings. Finally, the sample size of our study, which was sufficient for the analyses, may have limited the generalizability of our findings. Larger balanced sample sizes would provide greater statistical power and potentially reveal additional linked dimensions that were not detected in the present study. Despite these limitations, this study provides a valuable foundation for future research. The linked dimensions that we identified offer promising avenues for further investigation and could potentially serve as biomarkers to aid in improving diagnostic accuracy and formulating more targeted interventions for individuals with ASD.

Acknowledgements This study was supported by National Research Foundation (RS-2024-00408040), AI Graduate School Support Program (Sungkyunkwan University) (RS-2019-II190421), ICT Creative Consilience program (IITP-2025-RS-2020-II201821), and the Artificial Intelligence Innovation Hub program (RS-2021-II212068).

Author Contribution J.L. conceived the study, carried out the experiments, and wrote the draft. K.B. reviewed the manuscript and provided an analysis. S. K. reviewed the manuscript and provided an analysis. B.P. reviewed the manuscript and provided an analysis. H.P. provided supervision and funding.

Funding Open Access funding enabled and organized by SungKyunKwan University.

Data Availability No datasets were generated or analysed during the current study.

Declarations

Competing Interests The authors declare no competing interests.

References

Achenbach, T. M., & Rescorla, L. A. (2001). *Child Behavior Checklist for Ages 6–18* . https://doi.org/10.1037/t47452-000

Assaf, M., Jagannathan, K., Calhoun, V. D., Miller, L., Stevens, M. C., Sahl, R., O'Boyle, J. G., Schultz, R. T., & Pearlson, G. D. (2010). Abnormal functional connectivity of default mode sub-networks in autism spectrum disorder patients. *NeuroImage, 53*(1), 247–256. https://doi.org/10.1016/j.neuroimage.2010.05.067

Avants, B. B., Epstein, C. L., Grossman, M., & Gee, J. C. (2008). Symmetric diffeomorphic image registration with cross-correlation: Evaluating automated labeling of elderly and neurodegenerative brain. *Medical Image Analysis, 12*(1), 26–41. https://doi.org/10.1016/j.media.2007.06.004

Biswal, B., ZerrinYetkin, F., Haughton, V. M., & Hyde, J. S. (1995). Functional connectivity in the motor cortex of resting human brain using echo-planar mri. *Magnetic Resonance in Medicine, 34*(4), 537–541. https://doi.org/10.1002/mrm.1910340409

Bölte, S., Poustka, F., & Constantino, J. N. (2008). Assessing autistic traits: Cross-cultural validation of the social responsiveness scale (SRS). *Autism Research, 1*(6), 354–363. https://doi.org/10.1002/aur.49

Buch, A. M., Vértes, P. E., Seidlitz, J., Kim, S. H., Grosenick, L., & Liston, C. (2023). Molecular and network-level mechanisms explaining individual differences in autism spectrum disorder. N*ature Neuroscience, 26*, 650–663. https://doi.org/10.1038/s41593-023-01259-x

Cerliani, L., Mennes, M., Thomas, R. M., Di Martino, A., Thioux, M., & Keysers, C. (2015). Increased Functional Connectivity Between Subcortical and Cortical Resting-State Networks in Autism Spectrum Disorder. *JAMA Psychiatry, 72*(8), 767–777. https://doi.org/10.1001/jamapsychiatry.2015.0101

Chien, H.-Y., Lin, H.-Y., Lai, M.-C., Gau, S.S.-F., & Tseng, W.-Y.I. (2015). Hyperconnectivity of the Right Posterior Temporo-parietal Junction Predicts Social Difficulties in Boys with Autism Spectrum Disorder. *Autism Research, 8*(4), 427–441. https://doi.org/10.1002/aur.1457

Constantino, J. N. (2013). Social responsiveness scale. In F. R. Volkmar (Ed.) *Encyclopedia of autism spectrum disorders*. Springer. https://doi.org/10.1007/978-1-4419-1698-3_296

Constantino, J., & Gruber, C. P. (2005). *The social responsiveness scale (SRS) manual*. Los Angeles: Western Psychological Services.

Cox, R. W., & Hyde, J. S. (1997). Software tools for analysis and visualization of fMRI data. *NMR in Biomedicine, 10*(4–5), 171–178. https://doi.org/10.1002/(SICI)1099-1492(199706/08)10:4/5%3c171::AID-NBM453%3e3.0.CO;2-L

Di Martino, A., O'Connor, D., Chen, B., Alaerts, K., Anderson, J. S., Assaf, M., Balsters, J. H., Baxter, L., Beggiato, A., Bernaerts, S., Blanken, L. M. E., Bookheimer, S. Y., Braden, B. B., Byrge, L., Castellanos, F. X., Dapretto, M., Delorme, R., Fair, D. A., Fishman, I., & Milham, M. P. (2017). Enhancing studies of the connectome in autism using the autism brain imaging data exchange II. *Scientific Data, 4*(1), 1. https://doi.org/10.1038/sdata.2017.10

Dichter, G. S. (2012). Functional magnetic resonance imaging of autism spectrum disorders. *Dialogues in Clinical Neuroscience, 14*(3), 319–351. https://doi.org/10.31887/DCNS.2012.14.3/gdichter

Dickie, E. W., Anticevic, A., Smith, D. E., Coalson, T. S., Manogaran, M., Calarco, N., Viviano, J. D., Glasser, M. F., Van Essen, D. C., & Voineskos, A. N. (2019). Ciftify: A framework for surface-based analysis of legacy MR acquisitions. *NeuroImage, 197*, 818–826. https://doi.org/10.1016/j.neuroimage.2019.04.078

Esteban, O., Markiewicz, C. J., Blair, R. W., Moodie, C. A., Isik, A. I., Erramuzpe, A., Kent, J. D., Goncalves, M., DuPre, E., Snyder, M., Oya, H., Ghosh, S. S., Wright, J., Durnez, J., Poldrack, R. A., & Gorgolewski, K. J. (2019). fMRIPrep: A robust preprocessing pipeline for functional MRI. *Nature Methods, 16*(1), 1. https://doi.org/10.1038/s41592-018-0235-4

Fischl, B. (2012). FreeSurfer. *Neuroimage, 62*(2), 774–781. https://doi.org/10.1016/j.neuroimage.2012.01.021

Fleming, S. M., & Dolan, R. J. (2012). The neural basis of metacognitive ability. *Philosophical Transactions of the Royal Society b: Biological Sciences, 367*(1594), 1338–1349. https://doi.org/10.1098/rstb.2011.0417

Fortin, J.-P., Cullen, N., Sheline, Y. I., Taylor, W. D., Aselcioglu, I., Cook, P. A., Adams, P., Cooper, C., Fava, M., McGrath, P. J., McInnis, M., Phillips, M. L., Trivedi, M. H., Weissman, M. M., & Shinohara, R. T. (2018). Harmonization of cortical thickness measurements across scanners and sites. *NeuroImage, 167*, 104–120. https://doi.org/10.1016/j.neuroimage.2017.11.024

Gioia, G. A., Isquith, P. K., Guy, S. C., & Kenworthy, L. (2015). *Behavior Rating Inventory of Executive Function®, Second Edition (BRIEF®2, BRIEF2, BRIEF-2)*. https://doi.org/10.1037/t79467-000

Glasser, M. F., Sotiropoulos, S. N., Wilson, J. A., Coalson, T. S., Fischl, B., Andersson, J. L., Xu, J., Jbabdi, S., Webster, M., Polimeni, J. R., Van Essen, D. C., & Jenkinson, M. (2013). The minimal preprocessing pipelines for the Human Connectome Project. *NeuroImage, 80*, 105–124. https://doi.org/10.1016/j.neuroimage.2013.04.127

Greve, D. N., & Fischl, B. (2009). Accurate and robust brain image alignment using boundary-based registration. *NeuroImage, 48*(1), 63–72. https://doi.org/10.1016/j.neuroimage.2009.06.060

Hernandez, L. M., Rudie, J. D., Green, S. A., Bookheimer, S., & Dapretto, M. (2015). Neural Signatures of Autism Spectrum Disorders: Insights into Brain Network Dynamics. *Neuropsychopharmacology, 40*(1), 1. https://doi.org/10.1038/npp.2014.172

Hodges, H., Fealko, C., & Soares, N. (2020). Autism spectrum disorder: Definition, epidemiology, causes, and clinical evaluation. *Translational Pediatrics, 9*(Suppl 1), S55–S65. https://doi.org/10.21037/tp.2019.09.09

Hong, S.-J., Vos de Wael, R., Bethlehem, R. A. I., Lariviere, S., Paquola, C., Valk, S. L., Milham, M. P., Di Martino, A., Margulies, D. S., Smallwood, J., & Bernhardt, B. C. (2019). Atypical functional connectome hierarchy in autism. *Nature Communications, 10*(1), 1. https://doi.org/10.1038/s41467-019-08944-1

Hotelling, H. (1992). Relations Between Two Sets of Variates. In S. Kotz & N. L. Johnson (Eds.), *Breakthroughs in Statistics: Methodology and Distribution* (pp. 162–190). Springer. https://doi.org/10.1007/978-1-4612-4380-9_14

Hours, C., Recasens, C., & Baleyte, J.-M. (2022). ASD and ADHD Comorbidity: What Are We Talking About? *Frontiers in Psychiatry, 13*, 837424. https://doi.org/10.3389/fpsyt.2022.837424

Jones, T. B., Bandettini, P. A., Kenworthy, L., Case, L. K., Milleville, S. C., Martin, A., & Birn, R. M. (2010). Sources of group differences in functional connectivity: An investigation applied to autism spectrum disorder. *NeuroImage, 49*(1), 401–414. https://doi.org/10.1016/j.neuroimage.2009.07.051

Kennedy, D. P., & Courchesne, E. (2008). The intrinsic functional organization of the brain is altered in autism. *NeuroImage, 39*(4), 1877–1885. https://doi.org/10.1016/j.neuroimage.2007.10.052

Klein, A., Ghosh, S. S., Bao, F. S., Giard, J., Häme, Y., Stavsky, E., Lee, N., Rossa, B., Reuter, M., Neto, E. C., & Keshavan, A. (2017). Mindboggling morphometry of human brains. *PLOS Computational Biology, 13*(2), e1005350. https://doi.org/10.1371/journal.pcbi.1005350

Lai, M.-C., Kassee, C., Besney, R., Bonato, S., Hull, L., Mandy, W., Szatmari, P., & Ameis, S. H. (2019). Prevalence of co-occurring mental health diagnoses in the autism population: A systematic review and meta-analysis. *The Lancet Psychiatry, 6*(10), 819–829. https://doi.org/10.1016/S2215-0366(19)30289-5

Langs, G., Golland, P., & Ghosh, S. S. (2015). Predicting Activation Across Individuals with Resting-State Functional Connectivity Based Multi-Atlas Label Fusion. In N. Navab, J. Hornegger, W. M. Wells, & A. Frangi (Eds.), *Medical Image Computing and Computer-Assisted Intervention—MICCAI 2015* (pp. 313–320). Springer International Publishing. https://doi.org/10.1007/978-3-319-24571-3_38

Larivière, S., Paquola, C., Park, B., Royer, J., Wang, Y., Benkarim, O., Wael, R. V. de, Valk, S. L., Thomopoulos, S. I., Kirschner, M., Consortium, E., Lewis, L. B., Evans, A. C., Sisodiya, S. M., McDonald, C. R., Thompson, P. M., & Bernhardt, B. C. (2021). The ENIGMA Toolbox: Cross-disorder integration and multiscale neural contextualization of multisite neuroimaging datasets. *Nat Methods, 18*, 698–700. https://doi.org/10.1038/s41592-021-01186-4

Lau, W. K. W., Leung, M.-K., & Lau, B. W. M. (2019). Resting-state abnormalities in Autism Spectrum Disorders: A meta-analysis. *Scientific Reports, 9*(1), 1. https://doi.org/10.1038/s41598-019-40427-7

Liloia, D., Cauda, F., Uddin, L. Q., Manuello, J., Mancuso, L., Keller, R., Nani, A., & Costa, T. (2022). Revealing the selectivity of neuroanatomical alteration in autism spectrum disorder via reverse inference. *Biological Psychiatry: Cognitive Neuroscience and Neuroimaging, 8*, 1075. https://doi.org/10.1016/j.bpsc.2022.01.007

Lord, C., Rutter, M., & Le Couteur, A. (1994). Autism Diagnostic Interview—Revised: A revised version of a diagnostic interview for caregivers of individuals with possible pervasive developmental disorders. *Journal of Autism and Developmental Disorders, 24*(5), 659–685. https://doi.org/10.1007/BF02172145

Lord, C., Rutter, M., DiLavore, P. C., Risi, S., Gotham, K., & Bishop, S. (2012). *Autism Diagnostic Observation Schedule*. Second Edition.

Maenner, M. J. (2023). Prevalence and characteristics of autism spectrum disorder among children Aged 8 Years—autism and developmental disabilities monitoring Network, 11 Sites, United States, 2020. *MMWR Surveillance Summaries, 72*, 1. https://doi.org/10.15585/mmwr.ss7202a1

Marco, E. J., Khatibi, K., Hill, S. S., Siegel, B., Arroyo, M. S., Dowling, A. F., Neuhaus, J. M., Sherr, E. H., Hinkley, L. N. B., & Nagarajan, S. S. (2012). Children with autism show reduced somatosensory response: An MEG study. *Autism Research: Official Journal of the International Society for Autism Research, 5*(5), 340–351. https://doi.org/10.1002/aur.1247

Margulies, D. S., Ghosh, S. S., Goulas, A., Falkiewicz, M., Huntenburg, J. M., Langs, G., Bezgin, G., Eickhoff, S. B., Castellanos, F. X., Petrides, M., Jefferies, E., & Smallwood, J. (2016). Situating the default-mode network along a principal gradient of macroscale cortical organization. *Proceedings of the National Academy of Sciences, 113*(44), 12574–12579. https://doi.org/10.1073/pnas.1608282113

Di Martino, A., Yan, C.-G., Li, Q., Denio, E., Castellanos, F. X., Alaerts, K., Anderson, J. S., Assaf, M., Bookheimer, S. Y., Dapretto, M., Deen, B., Delmonte, S., Dinstein, I., Ertl-Wagner, B., Fair, D. A., Gallagher, L., Kennedy, D. P., Keown, C. L., Keysers, C., … Milham, M. P. (2014). The autism brain imaging data exchange: Towards a large-scale evaluation of the intrinsic brain architecture in autism. *Molecular Psychiatry*, *19*(6), 659–667. https://doi.org/10.1038/mp.2013.78

Masi, A., DeMayo, M. M., Glozier, N., & Guastella, A. J. (2017). An overview of autism spectrum disorder, heterogeneity and treatment options. *Neuroscience Bulletin, 33*(2), 183–193. https://doi.org/10.1007/s12264-017-0100-y

Massey, F. J. (1951). The Kolmogorov-Smirnov Test for Goodness of Fit. *Journal of the American Statistical Association, 46*(253), 68–78. https://doi.org/10.2307/2280095

Park, S., Haak, K. V., Cho, H. B., Valk, S. L., Bethlehem, R. A. I., Milham, M. P., Bernhardt, B. C., Di Martino, A., & Hong, S.-J. (2021). Atypical integration of sensory-to-transmodal functional systems mediates symptom severity in autism. *Frontiers in Psychiatry, 12*, 699813. https://doi.org/10.3389/fpsyt.2021.699813

Rasero, J., Jimenez-Marin, A., Diez, I., Toro, R., Hasan, M. T., & Cortes, J. M. (2023). The Nneurogenetics of functional connectivity alterations in autism: Insights from subtyping in 657 individuals. *Biological Psychiatry, 94*(10), 804–813. https://doi.org/10.1016/j.biopsych.2023.04.014

Robertson, C. E., & Baron-Cohen, S. (2017). Sensory perception in autism. *Nature Reviews Neuroscience, 18*(11), 11. https://doi.org/10.1038/nrn.2017.112

Schaefer, A., Kong, R., Gordon, E. M., Laumann, T. O., Zuo, X.-N., Holmes, A. J., Eickhoff, S. B., & Yeo, B. T. T. (2018). Local-Global Parcellation of the Human Cerebral Cortex from Intrinsic Functional Connectivity MRI. *Cerebral Cortex, 28*(9), 3095–3114. https://doi.org/10.1093/cercor/bhx179

Schulte-Rüther, M., Markowitsch, H. J., Fink, G. R., & Piefke, M. (2007). Mirror Neuron and Theory of Mind Mechanisms Involved in Face-to-Face Interactions: A Functional Magnetic Resonance Imaging Approach to Empathy. *Journal of Cognitive Neuroscience, 19*(8), 1354–1372. https://doi.org/10.1162/jocn.2007.19.8.1354

Shekhar, M., & Rahnev, D. (2018). Distinguishing the Roles of Dorsolateral and Anterior PFC in Visual Metacognition. *Journal of Neuroscience, 38*(22), 5078–5087. https://doi.org/10.1523/JNEUROSCI.3484-17.2018

Sparrow, S. S., & Cicchetti, D. V. (1989). The vineland adaptive behavior scales. In C. S. Newmark (Ed.), *Major psychological assessment instruments* (Vol. 2, pp. 199–231). Allyn & Bacon.

Thomas Yeo, B. T., Krienen, F. M., Sepulcre, J., Sabuncu, M. R., Lashkari, D., Hollinshead, M., Roffman, J. L., Smoller, J. W., Zöllei, L., Polimeni, J. R., Fischl, B., Liu, H., & Buckner, R. L. (2011). The organization of the human cerebral cortex estimated

by intrinsic functional connectivity. *Journal of Neurophysiology, 106*(3), 1125–1165. https://doi.org/10.1152/jn.00338.2011

Tustison, N. J., Avants, B. B., Cook, P. A., Zheng, Y., Egan, A., Yushkevich, P. A., & Gee, J. C. (2010). N4ITK: Improved N3 bias correction. *IEEE Transactions on Medical Imaging, 29*(6), 1310–1320. https://doi.org/10.1109/TMI.2010.2046908

Vasa, R. A., & Mazurek, M. O. (2015). An update on anxiety in youth with autism spectrum disorders. *Current Opinion in Psychiatry, 28*(2), 83–90. https://doi.org/10.1097/YCO.0000000000000133

Vos de Wael, R., Benkarim, O., Paquola, C., Lariviere, S., Royer, J., Tavakol, S., Xu, T., Hong, S.-J., Langs, G., Valk, S., Misic, B., Milham, M., Margulies, D., Smallwood, J., & Bernhardt, B. C. (2020). BrainSpace: A toolbox for the analysis of macroscale gradients in neuroimaging and connectomics datasets. *Communications Biology, 3*(1), 1. https://doi.org/10.1038/s42003-020-0794-7

Wichers, R. H., van der Wouw, L. C., Brouwer, M. E., Lok, A., & Bockting, C. L. H. (2023). Psychotherapy for co-occurring symptoms of depression, anxiety and obsessive-compulsive disorder in children and adults with autism spectrum disorder: A systematic review and meta-analysis. *Psychological Medicine, 53*(1), 17–33. https://doi.org/10.1017/S0033291722003415

Witten, D. M., Tibshirani, R., & Hastie, T. (2009). A penalized matrix decomposition, with applications to sparse principal components and canonical correlation analysis. *Biostatistics, 10*(3), 515–534. https://doi.org/10.1093/biostatistics/kxp008

Xia, C. H., Ma, Z., Ciric, R., Gu, S., Betzel, R. F., Kaczkurkin, A. N., Calkins, M. E., Cook, P. A., García de la Garza, A., Vandekar, S. N., Cui, Z., Moore, T. M., Roalf, D. R., Ruparel, K., Wolf, D. H., Davatzikos, C., Gur, R. C., Gur, R. E., Shinohara, R. T., … Satterthwaite, T. D. (2018). Linked dimensions of psychopathology and connectivity in functional brain networks. *Nature Communications, 9*, 3003. https://doi.org/10.1038/s41467-018-05317-y

Yahata, N., Morimoto, J., Hashimoto, R., Lisi, G., Shibata, K., Kawakubo, Y., Kuwabara, H., Kuroda, M., Yamada, T., Megumi, F., Imamizu, H., Náñez, J. E., Sr., Takahashi, H., Okamoto, Y., Kasai, K., Kato, N., Sasaki, Y., Watanabe, T., & Kawato, M. (2016). A small number of abnormal brain connections predicts adult autism spectrum disorder. *Nature Communications, 7*(1), 11254. https://doi.org/10.1038/ncomms11254

Zhang, Y., Brady, M., & Smith, S. (2001). Segmentation of brain MR images through a hidden Markov random field model and the expectation-maximization algorithm. *IEEE Transactions on Medical Imaging, 20*(1), 45–57. https://doi.org/10.1109/42.906424

Zhuang, X., Yang, Z., & Cordes, D. (2020). A technical review of canonical correlation analysis for neuroscience applications. *Human Brain Mapping, 41*(13), 3807–3833. https://doi.org/10.1002/hbm.25090